V. NEIMASH,[1] G. DOVBESHKO,[1] P. SHEPELYAVYI,[2] V. DANKO,[2] V. MELNYK,[3]
M. ISAIEV,[3] A. KUZMICH[3]

[1] Institute of Physics, Nat. Acad. of Sci. of Ukraine
  (46, Nauky Ave., Kyiv 03028, Ukraine; e-mail: neimash@gmail.com)
[2] V.E. Lashkaryov Institute of Semiconductor Physics, Nat. Acad. of Sci. of Ukraine
  (41, Nauky Ave, Kyiv 03028, Ukraine)
[3] Taras Shevchenko National University of Kyiv, Faculty of Physics
  (64/13, Volodymyrs'ka Str., Kyiv 01601, Ukraine)

RAMAN SCATTERING
IN THE PROCESS OF TIN-INDUCED
CRYSTALLIZATION OF AMORPHOUS SILICON

Metal-induced crystallization in Si–Sn–Si thin film structures has been studied, by using the Raman scattering at various light powers. The Raman spectra are used to monitor the temperature, size, and concentration of Si crystals formed in the amorphous Si matrix. A significant acceleration of the metal-induced crystallization in Si–Sn–Si structures at their laser-assisted annealing in comparison with their annealing in dark is revealed. A basic possibility of the "on line" monitoring of the size and the concentration of Si nanocrystals in the course of their formation is demonstrated.

K e y w o r d s: solar cell, thin films, nanocrystals, silicon, tin, metal-induced crystallization.

1. Introduction

A film composite consisting of Si nanocrystals in an amorphous Si matrix (nc-Si) is considered to be a promising material for the next generation of quantum-dot solar cells (SCs) [1]. It is so because this composite has a unique set of physical properties: the direct-band-gap mechanism of light absorption, the dependence of the energy gap width on the nanocrystal size, the stability to the Staebler–Wronski effect, and a capability to be formed on flexible substrates.

The application of nanocomposite silicon makes it possible to substantially enhance the SC efficiency by creating cascade polymorphic heterostructures [2, 3] and to reduce the SC manufacture cost due to the advantages of the thin-film and roll-to-roll technologies [4, 5]. The main obstacles hampering the implementation of nc-Si advantages into practice include an insufficient development of technologies aimed at the exact control over the size and the concentration of Si nanocrystals at the economically efficient rates of formation of films. Therefore, despite a considerable number of available techniques for the nc-Si manufac-

ture, a lot of attention is paid to their improvement, as well as to the development of new ones (see, e.g., works [6–12]).

One of the promising ways in this direction is the application of the metal-induced crystallization (MIC) in amorphous silicon [13–17]. In particular, a capability of forming Si crystals with dimensions of 2–5 nm and a volume fraction reaching up to 80% in an amorphous Si matrix with the use of the low-temperature tin-stimulated crystallization in amorphous Si has been demonstrated recently [18–20]. The corresponding experimental results were interpreted with the help of a new MIC mechanism proposed in works [20, 21], which considerably differs from other mechanisms known for other metals [13, 15–17]. According to the new one, silicon nanocrystals are formed as a result of the cyclic repetition of the formation and the decay of a supersaturated silicon solution in tin that occur in a narrow eutectic layer at the a-Si/Sn interface between tin microdroplets located in the bulk of amorphous Si. In this work, we show that the tin-induced crystallization of amorphous silicon can be stimulated by laser light with a relatively low intensity. This circumstance allows one to measure the temperature, size, and concentration of nanocrystals with the help of the Raman scattering in the
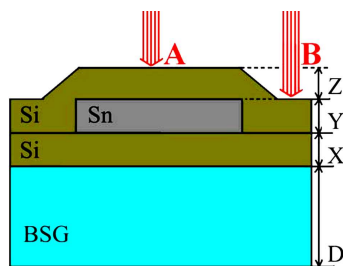
X; Y; Z = 50 ÷ 200 nm;   D = 1mm

Fig. 1. Schematic representation of the cross-sections of the layered Si–Sn–Si structures under study

course of nanocrystal formation and, simultaneously, to control the crystallization process by varying the intensity of a laser irradiation and its duration.

2. Experimental Part

We studied layered film structures, whose cross-section is schematically shown in Fig. 1. The specimens were fabricated by alternatively depositing silicon and tin thermally evaporated in vacuum. The metals were deposited onto borosilicate glass substrates 76×76 mm^2 in dimensions and heated to a temperature of about 150 °C, by using the following procedure:

• first, a layer of amorphous silicon (a-Si) of the thickness X was deposited onto the whole substrate area;

• then, a spot (a layer) of metallic tin of the thickness Y was deposited onto the a-Si layer through a mask 50 mm in diameter;

• finally, another layer of amorphous Si of the thickness Z was deposited onto the indicated layers and over the whole substrate area.

The values of the parameters X, Y, and Z were discretely changed within an interval of 50–200 nm with a step of 50 nm. All three deposition stages were carried out in the same vacuum chamber, not allowing a decompression, and at a residual pressure of 10^{-3} Pa by consecutively applying three different evaporators. Si (99.999%) and Sn (99.92%) targets were sputtered. Specimens with various $X : Y : Z$ ratios were studied.

The specimens fabricated with the use of the described procedure can be regarded as a macroscopic model analog of microscopic metallic Sn droplets in the amorphous Si environment. Such a configuration

can be observed in Si–Sn film alloys and gives rise to the crystallization in the surrounding silicon regions [20].

Raman spectra were measured on a Renishaw micro-Raman spectrometer. Their excitation was carried out by a laser with a wavelength of 633 nm and the maximum power of a light flux $I_0 = 10$ mW. The diameter of a laser beam was equal to 1 or 2 μm, which provided the density of a light flux of up to 3×10^5 W/cm^2. The Raman spectra were measured at room temperature in two characteristic regions of the specimen surface (see Fig. 1): region A (above the Sn film) and region B (beyond the Sn film). The spectrum scanning time and, accordingly, the duration of the laser beam action on the specimen amounted to 30 s. Raman spectra were registered at the same place of the specimen at various laser excitation powers in the following sequence: (i) $I_1 = 0.1I_0$, (ii) $I_2 = 0.5I_0$, (iii) $I_3 = I_0$, and (iv) $I_4 = 0.1I_0$ again. Some specimens were used for the multiple registration of Raman spectra at the same place and provided the same power of laser irradiation in order to analyze the role of the laser treatment duration.

3. Results and Their Discussion

The spectra of Raman scattering by longitudinal optical (LO) phonons measured in an interval of 300–600 cm^{-1} in region B for all specimens (Fig. 1) and at any power of Raman scattering excitation by a laser beam up to the maximum value contain only a wide band of amorphous silicon with a maximum at 475 cm^{-1} [22]. At the same time, in the spectra for region A (above the layer of metallic tin), besides the band of amorphous silicon state at $I_2 = 0.5I_0$, there arises and grows, at $I_3 = I_0$, an additional narrow band in the interval 490–500 cm^{-1}, which corresponds to the nanocrystalline phase of silicon [22, 23]. The latter band survives in further measurements carried out at the lower irradiation power $I_4 = 0.1I_0$ only for the same section A of the specimen. This fact is illustrated in Fig. 2, where the evolution of the Raman spectrum, when the laser excitation power first increases (panel a) and then decreases (panel b), is depicted on the same scale. In other words, at the laser beam powers I_2 and I_3 of the Raman scattering excitation, silicon nanocrystals are formed in region A.

Note that the crystallization of amorphous Si under the action of a laser irradiation was observed by
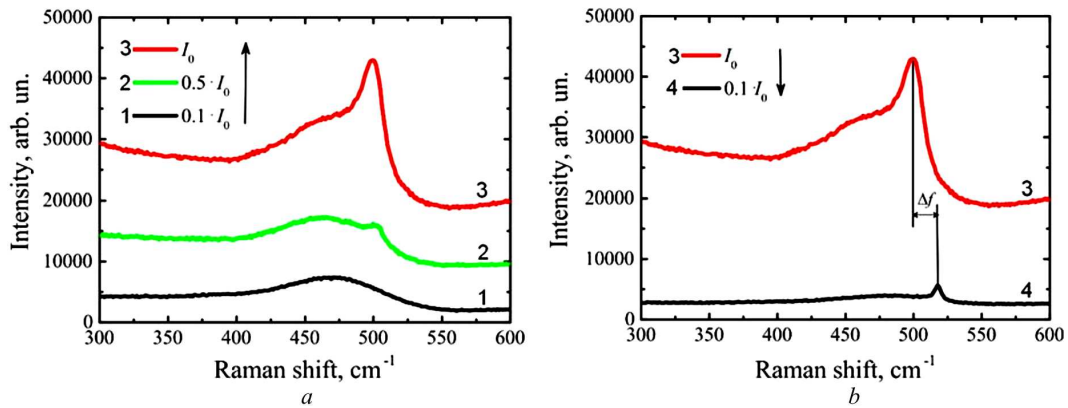
Fig. 2. Raman spectra of the surface region A registered for the sequence of growing (a) and decreasing (b) light intensities: $I = I_1$ (1), I_2 (2), I_3 (3), and I_4 (4). A specimen with $X:Y:Z = 100:50:100$
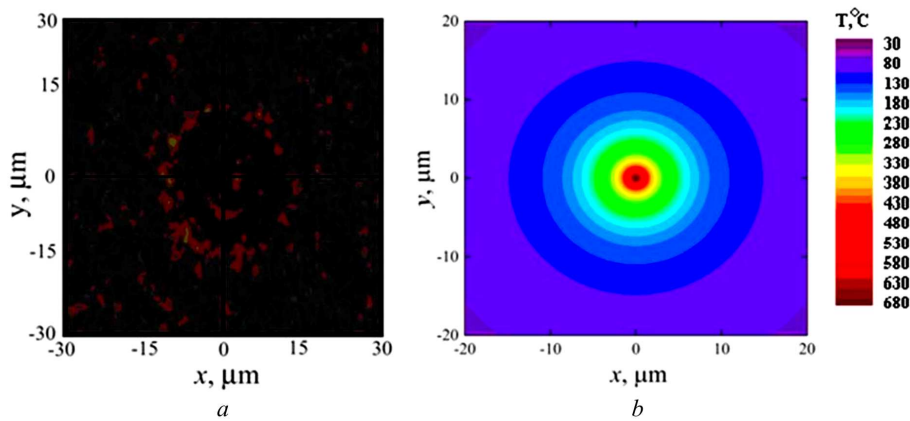

Fig. 3. Optical microscopic image of the mark of the excitation laser action on the specimen surface (a); the calculated equilibrium distribution of the specimen surface temperature for the specimen with $X:Y:Z = 100:100:100$ and at $I = I_0$ (b)

a lot of researchers [24–29]. It is agreed that, after a local heating of a-Si by a laser beam to temperatures higher than 1000 °C [24–26] or the so-called "cold melting" of Si under the influence of short, but powerful laser pulses ($10^{11} \div 10^{12}$ W/cm^2) [27–29], a thermally induced crystallization takes place. However, in our case, the power of a laser beam was insufficient for the thermal crystallization. This fact is evidenced by the absence of the Raman band corresponding to crystalline silicon in region B of specimens even after three scans of the spectrum at the maximum power of exciting light.

The appearance of this band in region A is evidently associated with the presence of the tin layer, which considerably reduces the temperature of a-Si crystallization [18, 19] following the MIC mechanism. At the Si/Sn interface, this mechanism is real-

ized at temperatures above the melting point of Sn (about 230 °C) [20, 21], which is confirmed by the fact that the appearance of the Raman band corresponding to the crystalline Si phase is accompanied by a variation in the specimen surface relief at the place of the laser beam action, probably owing to the fusion of the tin layer. A typical mark of the laser beam action on the specimen surface observed through an optical microscope of the targeting device of the Raman installation is shown in Fig. 3, a. One can see that its size can exceed the diameter of an exciting laser beam by almost an order of magnitude. Outside the mark, the Raman spectrum (at $I = 0.1I_0$) does not contain the band of crystalline Si. For specimens with different ratios $X:Y:Z$, the diameter of the mark, its pattern, and its contrast are somewhat different at identical intensities and durations of the
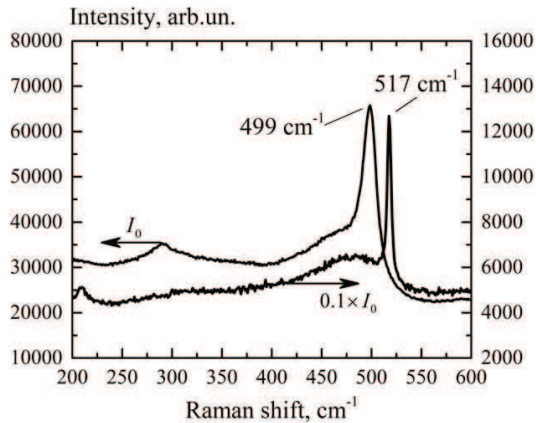
Fig. 4. Temperature-induced shift of the crystalline-phase band. Raman spectra were registered at $I = I_0$ (*1*) and $0.1I_0$ (*2*). $X : Y : Z = 100 : 200 : 100$

laser light action. Probably, this fact may be associated with different conditions of light absorption and heat removal at different layer thicknesses in the examined structures. Ultimately, those factors govern the temperature distribution in the region illuminated with a laser beam and around it. Figure 3, *b* demonstrates the results of calculation of the equilibrium temperature distribution over the surface of a specimen with $X : Y : Z = 100 : 100 : 100$ (in nm) around the axis of a laser beam 1 μm in diameter and with $I = I_0$. The model proposed in work [30] was used in calculations. One can see that the maximum heating temperature at the center of a light spot can reach 680 °C.

Slightly higher values were obtained, when estimating the surface temperature of this specimen in the area of laser beam action according to the thermal shift of the frequency at the maximum of the Raman band corresponding to the crystalline phase. The Raman band of crystalline silicon is known to have a maximum at the frequency $f_c = 520$ cm^{-2} at room temperature and to shift toward lower energies by the value Δf_T proportional to the elevation of the crystal temperature [31–33]. We also experimentally observed a low-frequency shift of the Raman peak by the crystalline Si phase as the intensity of laser irradiation grew. The peak of the as-formed crystalline phase shifted toward higher energies when the laser light power decreased from I_0 to $0.1I_0$ (Fig. 2, *b*).

In Fig. 4, the Raman spectra of the specimen with $X : Y : Z = 100 : 200 : 100$ registered first at $I = I_0$ and

then at $I = 0.1I_0$ are shown on the scales different by an order of magnitude.

A further reduction of the laser excitation intensity by an order of magnitude – within the limits of $(0.01 \div 0.1)I_0$ – does not appreciably affect the band position. This means that light of such power does not heat up the specimens substantially in comparison with room temperature. Therefore, we may assert that the value of Δf_T at $I > 0.1I_0$ characterizes the growth of the specimen temperature at the place of the Raman spectrum measurement with respect to room one owing to the local heating by the laser light.

The application of the experimental temperature dependence of the Raman peak shift for the crystalline Si peak from work [33] makes it possible to estimate the local temperature in the region of laser irradiation actions. In specimens with different $X : Y : Z$ ratios, it varies in the interval from 350 to 960 °C ($\Delta f_T = 8 \div 22$ cm^{-1}) at $I = I_0$, being approximately identical over every specimen. It is evident that the thicknesses and the ratios between the thicknesses of a-Si and Sn layers govern the conditions of laser light absorption and heat removal and, accordingly, the degree of structure heating.

It should be noted that the dependence obtained in work [33] for Si single crystals can be applied to nanocrystals, as in our case, only as a rough one. For the Raman spectroscopy to be correctly applied in the temperature measurement of materials with silicon nanocrystals, it is necessary to know the dependences $\Delta f_T(\Delta T)$ for nc-Si with various dimensions of crystallites.

The vibrational spectrum of nanoparticles depends on their dimensions. Therefore, the Raman spectroscopy has already been used for the determination of particle dimensions for rather a long time [22, 23, 34, 35]. In particular, if Si crystals are smaller than 20 nm in diameter, the peak in the Raman band of LO-phonon shifts from 520 cm^{-1} toward lower energies by a value of Δf_R. In Fig. 5, the dependence of this shift on the crystal size, $\Delta f_R(\Delta R)$, measured at room temperature [35] is plotted.

As is seen from Fig. 4, the peak frequency of the crystalline Si phase (517 cm^{-1}) in the Raman spectrum measured at $I = 0.1I_0$ (i.e. at room temperature of the specimen) is by $\Delta f_T = 3$ cm^{-1} lower than the peak frequency of single-crystalline Si (520 cm^{-1}) at the same temperature. According to Fig. 5, this

fact means that crystallites about 4.5 nm in size dominate in the as-formed crystal phase. In the specimens with other $X:Y:Z$ ratios, the dimensional shift Δf_R changes within the interval of 2–12 cm^{-1}, which corresponds to the interval of crystallite dimensions from 2 to 6 nm. Just this interval is of practical interest from the viewpoint of the nanosilicon application to solar cells as a direct-band-gap film material with a controllable energy gap width.

The volume fraction of the amorphous-crystalline composite occupied by nanocrystals, X_C, can be determined from the relation between the integrated intensities of Raman bands corresponding to the crystalline and amorphous phases [34]. Figure 6 demonstrates how this phase relation changes with the number of 30-s scans of the Raman spectrum at the same place of the specimen. One can see that, for every next scan, the amplitude of the crystalline phase band grows, i.e. nanocrystals are accumulated in the course of the tin-induced crystallization of a-Si heated by laser light. In particular, in the 50:100:200 specimen, X_C becomes stabilized at a level of 92% at the fifth scan, i.e. after the 2.5-min interval of the laser treatment. In the specimens where the thickness of the external a-Si layer did not exceed 100 nm, X_C reached a level of 90% already in the course of the first scan, i.e. within 30 s. The corresponding crystallization rate turned out by an order of magnitude higher than that observed in similar structures thermally treated at 300–400 °C in dark [21]. If this effect had been associated only with a higher temperature in the region of the laser beam action, then, according to work [17], the size of crystallites, R, would have been considerably larger than 5 nm. However, this is not the case. We may assume that the MIC becomes accelerated in the external a-Si layer owing to a strong photoionization of silicon by powerful laser light. It is so, because the dissolution of amorphous silicon in liquid tin at the interface between the layers becomes substantially facilitated owing to the screening of covalent silicon bonds by free electrons and the formation of additional dangling bonds [36]. A verification of this assumption demands additional researches. However, irrespective of the mechanism of MIC acceleration by laser light, it can be used for a controllable formation of nanocrystals in layered Si–Sn film structures.

The results of our measurements and estimations obtained for some characteristic specimens with a fi-
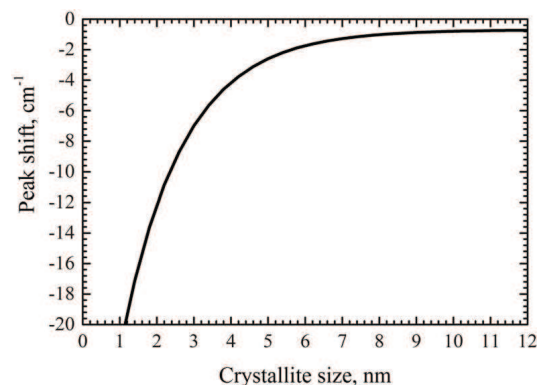

Fig. 5. Dependence $\Delta f_R(R)$ of the shift of the Raman peak for the nanocrystalline Si phase with respect to the peak of single-crystalline Si at 520 cm^{-1} on the crystallite size R [35]
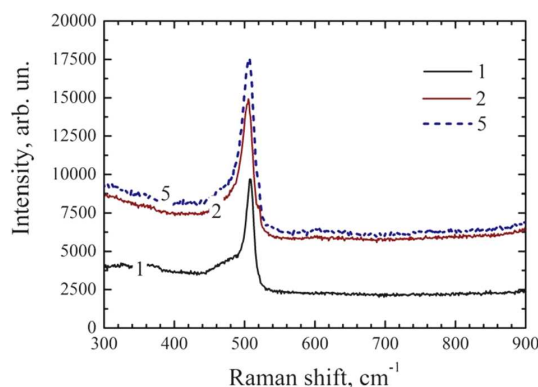

Fig. 6. Raman spectra for the specimen with $X:Y:Z = 50:100:200$ at $I = I_0$ registered after the first (*1*), second (*2*), and fifth scan (*5*) at the same place of the specimen surface

nal content of the crystalline phase more than 80% and crystallite dimensions not exceeding 5 nm are presented in Table. The thicknesses (X, Y, Z) of layers in nanometer units are indicated in the second column of the table. The third column contains the positions of the Raman peak corresponding to the crystalline phase at the laser excitation power $I = 0.1I_0$, i.e. at room temperature, and at the increased power $I = kI_0$. The corresponding values of the coefficient k are shown in the fourth column. The next columns contain the following quantities: the temperature-induced shift Δf_T of the crystal phase peak, the approximate [30] temperature T (in °C units) at the laser action region and Raman spectrum measurements, the number of 30-s scans of the Raman spectrum, when the specimen is subjected to

Ratio of the thicknesses of layers $X:Y:Z$	Position of the Raman peak of the crystal phase ω, cm^{-1} for various intensities $(0.1I_0)/(kI_0)$	Power change coefficient k	Temperature shift of the crystal phase peak $\Delta\omega_T$, cm^{-1}	Temperature at the laser action place T, °C	Number of (30-s) scans of the Raman spectrum	Dimensional shift of the position of the crystal phase peak $\Delta\omega_R$, cm^{-1}	Dominant size of crystallites R, nm	Volume fraction of the crystal phase X_C, %
50 : 100 : 200	508/502	0.5	6	250	5	12	1.9	92
100 : 100 : 100	516/494	1.0	22	960	1	4	3.5	90
100 : 100 : 200	511/500	0.5	11	480	1	9	2.2	92
100 : 200 : 100	517.5/498	1.0	19.5	850	1	2.5	5.0	86
150 : 100 : 50	517/497	1.0	20	870	1	3	4.3	81
200 : 200 : 200	517/497	1.0	22	960	5	3	4.3	80

the laser beam action, the size-induced shift Δf_R of the crystal phase peak at room temperature with respect to the peak position for single-crystalline silicon ($f_C = 520$ cm^{-1}), and the estimated values (using the technique of works [22, 23, 34]) for the dominant crystallite size R and the volume fraction X_C occupied by them.

From the table, one can see that, while studying three-layer Si–Sn–Si film structures and measuring the Raman spectra excited by a light flux with a power density of 3×10^5 W/cm^2, the specimen surface becomes heated up substantially. The heating temperature can reach several hundreds of degrees, which is determined (a) by the power and diameter of the excitation laser beam and (b) by the conditions of light absorption and heat removal depending on the thicknesses of structure layers.

At temperatures above the tin melting point, amorphous silicon is dissolved in liquid tin and afterward precipitates from the solution in the form of nanocrystals. This mechanism of MIC was described in work [21] in detail. From Table, one can see that the size of Si nanocrystals and their concentration depend on the temperature and duration of the process and, accordingly, on the power and time of the laser light action. The measurement and the analysis of the Raman spectrum excited by laser light in the course of the tin-induced transformation of silicon from the amorphous state into the crystalline one make it possible to determine – and, modulating the laser power, to control – the size of crystallites and the volume fraction occupied by them in the "on-line" mode. The number and the thicknesses of initial a-Si and Sn layers can be technological factors determining the total thickness of the amorphous-crystalline composite film, the distribution of parameters of the nanocrystalline phase over the film, as well as the amount and the state of residual tin.

4. Conclusions

To summarize, the application of laser radiation to provide conditions for the tin-induced crystallization in amorphous silicon and, simultaneously, to measure the size and concentration of formed nanocrystals with the use of Raman spectroscopy can form a basis for a new technology aimed at the quality control in the course of fabrication of nanocrystalline silicon films with a given energy gap width, in particular, for solar cells of the cascade type. A substantial acceleration of the crystallization of amorphous Si, induced by tin, its heating by laser radiation in comparison with the heating in dark, which was revealed in this work, can testify to a considerable role of the ionization in MIC processes.

1. M.C. Beard, J.M. Luther, and A.J. Nozik, Nat. Nano **9**, 951 (2014).
2. Z.I. Alferov, V.M. Andreev, and V.D. Rumyantsev, Semiconductors **38**, 899 (2004).
3. B. Yan, G. Yue, X. Xu, J. Yang, and S. Guha, Phys. Status Solidi A **207**, 671 (2010).
4. N.S. Lewis, Science **315**, 798 (2007).
5. R. Søndergaard, M. Hösel, D. Angmo, T.T. Larsen-Olsen, and F.C. Krebs, Mater. Today **15**, 36 (2012).
6. M. Birkholz, B. Selle, E. Conrad, K. Lips, and W. Fuhs, J. Appl. Phys. **88**, 4376 (2000).
7. B. Rech, T. Roschek, J. Müller, S. Wieder, and H. Wagner, Sol. Energy Mater. Sol. Cells **66**, 267 (2001).
8. M.K. van Veen, C.H.M. van der Werf, and R.E.I. Schropp, J. Non-Cryst. Solids **338–340**, 655 (2004).

9. Y. Mai, S. Klein, R. Carius, H. Stiebig, L. Houben, X. Geng, and F. Finger, J. Non-Cryst. Solids **352**, 1859 (2006).

10. H. Li, R.H. Franken, R.L. Stolk, C.H.M. van der Werf, J.K. Rath, and R.E.I. Schropp, J. Non-Cryst. Solids **354**, 2087 (2008).

11. R. Amrani, F. Pichot, L. Chahed, and Y. Cuminal, Cryst. Struct. Theory Appl. **1**, 57 (2012).

12. G. Fugallo and A. Mattoni, Phys. Rev. B **89**, 045301 (2014).

13. O. Nast and A.J. Hartmann, J. Appl. Phys. **88**, 716 (2000).

14. M. Jeon, C. Jeong, and K. Kamisako, Mater. Sci. Technol. **26**, 875 (2010).

15. M.A. Mohiddon and M.G. Krishna, J. Mater. Sci. **47**, 6972 (2012).

16. D. Van Gestel, I. Gordon, and J. Poortmans, Sol. Energy Mater. Sol. Cells **119**, 261 (2013).

17. A. Mohiddon and G. Krishna, in *Crystallization – Science and Technology*, edited by A. Marcello (InTech, 2012), p. 461.

18. V.V. Voitovych, V.B. Neimash, N.N. Krasko, A.G. Kolosiuk, V.Y. Povarchuk, R.M. Rudenko, V.A. Makara, R.V. Petrunya, V.O. Juhimchuk, and V.V. Strelchuk, Semiconductors **45**, 1281 (2011).

19. V.B. Neimash, V.M. Poroshin, A.M. Kabaldin, V.O. Yukhymchuk, P.E. Shepelyavyi, V.A. Makara, and S.Y. Larkin, Ukr. J. Phys. **58**, 865 (2013).

20. V. Neimash, V. Poroshin, P. Shepeliavyi, V. Yukhymchuk, V. Melnyk, A. Kuzmich, V. Makara, and A.O. Goushcha, J. Appl. Phys. **114**, 213104 (2013).

21. V.B. Neimash, A.O. Goushcha, P.E. Shepeliavyi, V.O. Yukhymchuk, V.A. Dan'ko, V.V. Melnyk, and A.G. Kuzmich, Ukr. J. Phys. **59**, 1168 (2014).

22. H. Richter, Z.P. Wang, and L. Ley, Solid State Commun. **39**, 625 (1981).

23. I.H. Campbell and P.M. Fauchet, Solid State Commun. **58**, 739 (1986).

24. S. Chen and I.C. Hsleh, Solid State Technol. **39**, 113 (1996).

25. A.A.D.T. Adikaari and S.R.P. Silva, J. Appl. Phys. **97**, (2005).

26. T.Y. Choi, D.J. Hwang, and C.P. Grigoropoulos, Opt. Eng. **42**, 3383 (2003).

27. J.-M. Shieh, Z.-H. Chen, B.-T. Dai, Y.-C. Wang, A. Zaitsev, and C.-L. Pan, Appl. Phys. Lett. **85**, 1232 (2004).

28. V.A. Volodin and A.S. Kachko, Semiconductors **45**, 265 (2011).

29. A.V. Emelyanov, A.G. Kazanskii, P.K. Kashkarov, O.I. Konkov, E.I. Terukov, P.A. Forsh, M.V. Khenkin, A.V. Kukin, M. Beresna, and P. Kazansky, Semiconductors **46**, 749 (2012).

30. P.J. Newby, B. Canut, J.-M. Bluet, S. Gomès, M. Isaiev, R. Burbelo, K. Termentzidis, P. Chantrenne, L.G. Fréchette, and V. Lysenko, J. Appl. Phys. **114**, 014903 (2013).

31. M. Balkanski, R.F. Wallis, and E. Haro, Phys. Rev. B **28**, 1928 (1983).

32. B. Stoib, S. Filser, N. Petermann, H. Wiggers, M. Stutzmann, and M.S. Brandt, Appl. Phys. Lett. **104**, 161907 (2014).

33. S. Périchon, V. Lysenko, B. Remaki, D. Barbier, and B. Champagnon, J. Appl. Phys. **86**, 4700 (1999).

34. E. Bustarret, M.A. Hachicha, and M. Brunel, Appl. Phys. Lett. **52**, 1675 (1988).

35. W. Cheng and S.-F. Ren, Phys. Rev. B **65**, 205305 (2002).

36. A. Hiraki, *Low Temperature Reactions at Si/metal Interfaces; What Is Going on at the Interfaces?* (North-Holland, Amsterdam, 1984).

В.Б. Неймаш, Г.І. Довбешко, П.Є. Шепелявий,
В.А. Данько, В.В. Мельник, М.В. Ісаєв, А.Г. Кузьмич

КОМБІНАЦІЙНЕ РОЗСІЮВАННЯ
СВІТЛА В ПРОЦЕСІ ІНДУКОВАНОЇ ОЛОВОМ
КРИСТАЛІЗАЦІЇ АМОРФНОГО КРЕМНІЮ

Р е з ю м е

Методом комбінаційного розсіювання світла різної потужності поверхнею тонкоплівкових структур Si–Sn–Si досліджено процеси індукованої оловом кристалізації аморфного кремнію. Аналіз спектрів комбінаційного розсіювання використано для контролю температури, розміру та концентрації кристалів Si, що утворюються в матриці аморфного Si в процесі вимірювання спектрів. Виявлено значне прискорення металом індукованої кристалізації при лазерному відпалі структур Si–Sn–Si порівняно з відпалом у темряві. Показано принципову можливість контролю в режимі "on line" розмірів і концентрації кристалів Si в процесі їх формування.